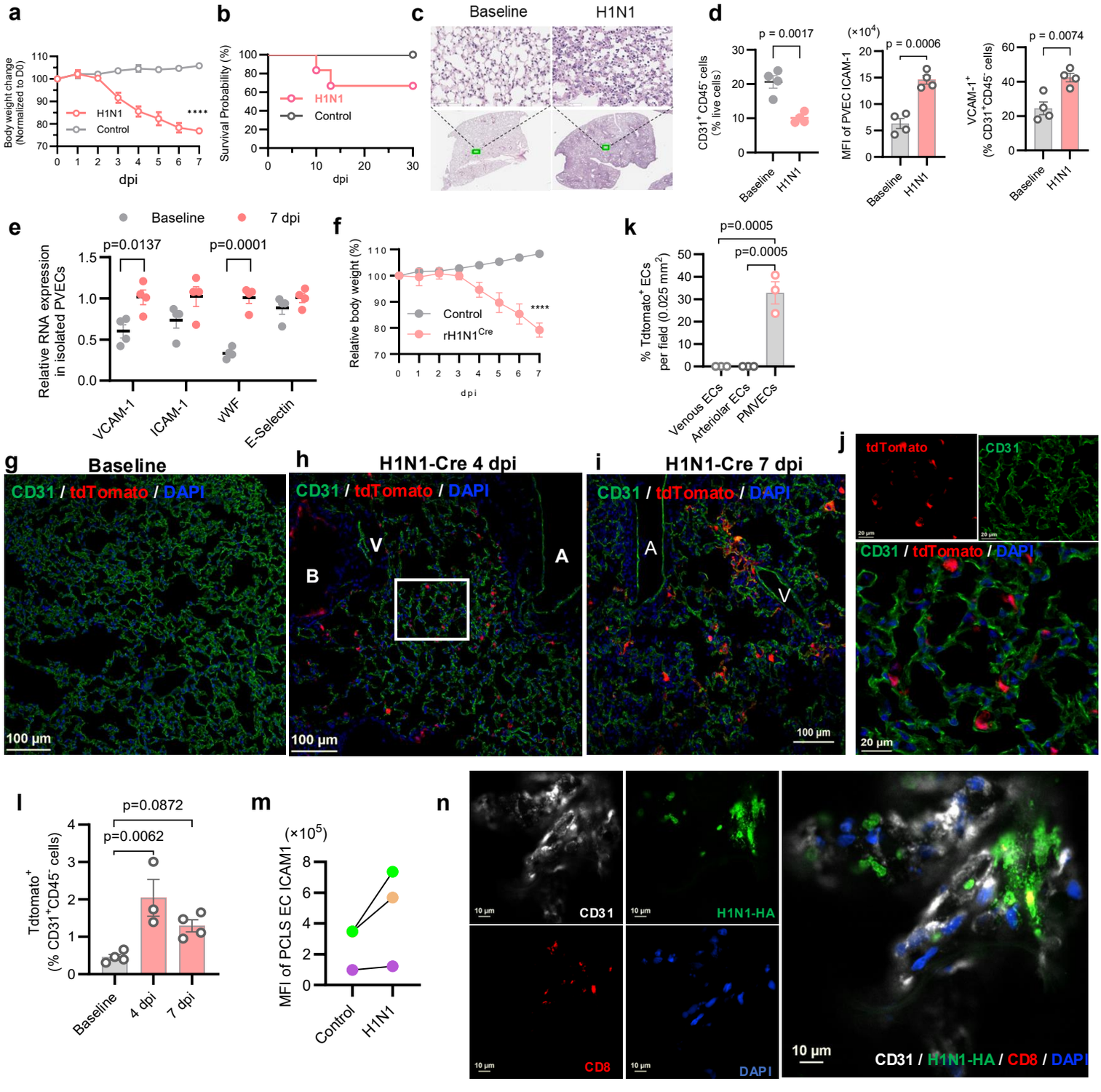

Extended Data Figure 1. H1N1 infection induces endothelial activation and MHC-I upregulation. (**a-e**) C57BL/6 mice were inoculated with 100 PFU H1N1 (A/PR/8/1934), with uninfected mice as control. (**a**) Body weight, (**b**) survival curve, (**c**) H & E staining of lung section at 7 dpi. **(d)** Flow cytometry of PVEC numbers at baseline and 7 dpi, and adhesion molecule (ICAM-1 MFI, %VCAM-1$^+$ ECs). (**e**) RT-qPCR analysis of *VCAM1, ICAM1, vWF, and E-selectin* in isolated PVECs at baseline and 7 dpi, normalized to *GAPDH*. (**f-l**) tdTomato reporter mice were inoculated with 100 PFU rH1N1^{Cre}. Lungs were perfused, harvested, and fixed at 7 dpi; uninfected mice served as controls. (**f**) Body weight . (**g-j**) Confocal images of lung sections stained for CD31 at baseline (**g**), 4 dpi (**h**), and 7 dpi (**i**), as well as (**j**) zoom area in **h**. A: Arteriole, V: Venule, B: Bronchus. (**k**) Quantification of infected ECs (tdTomato$^+$CD31$^+$) in microvasculature, arteriole and Venule of infected areas at 7 dpi. (**l**) Flow cytometry of infected ECs (% tdTomato$^+$CD31$^+$CD45$^-$ of CD31$^+$CD45$^-$ cells) at baseline, 4 and 7 dpi. . (**m-n**) Human PCLSs were infected with H1N1 (1x10^5 PFU) for 2 days. (**m**) ICAM1 MFI on PMVECs from three donors (different colors) by flow cytometry. (**n**) Representative confocal images of CD31, H1N1-HA, and CD8$^+$ T cells. All quantitative data are presented as mean ± s.e.m. from at least three independent biological replicates (mice). Data are mean ± s.e.m. Statistical analysis by unpaired two-tailed t-tests (d-e, m) and one-way ANOVA (k-i).

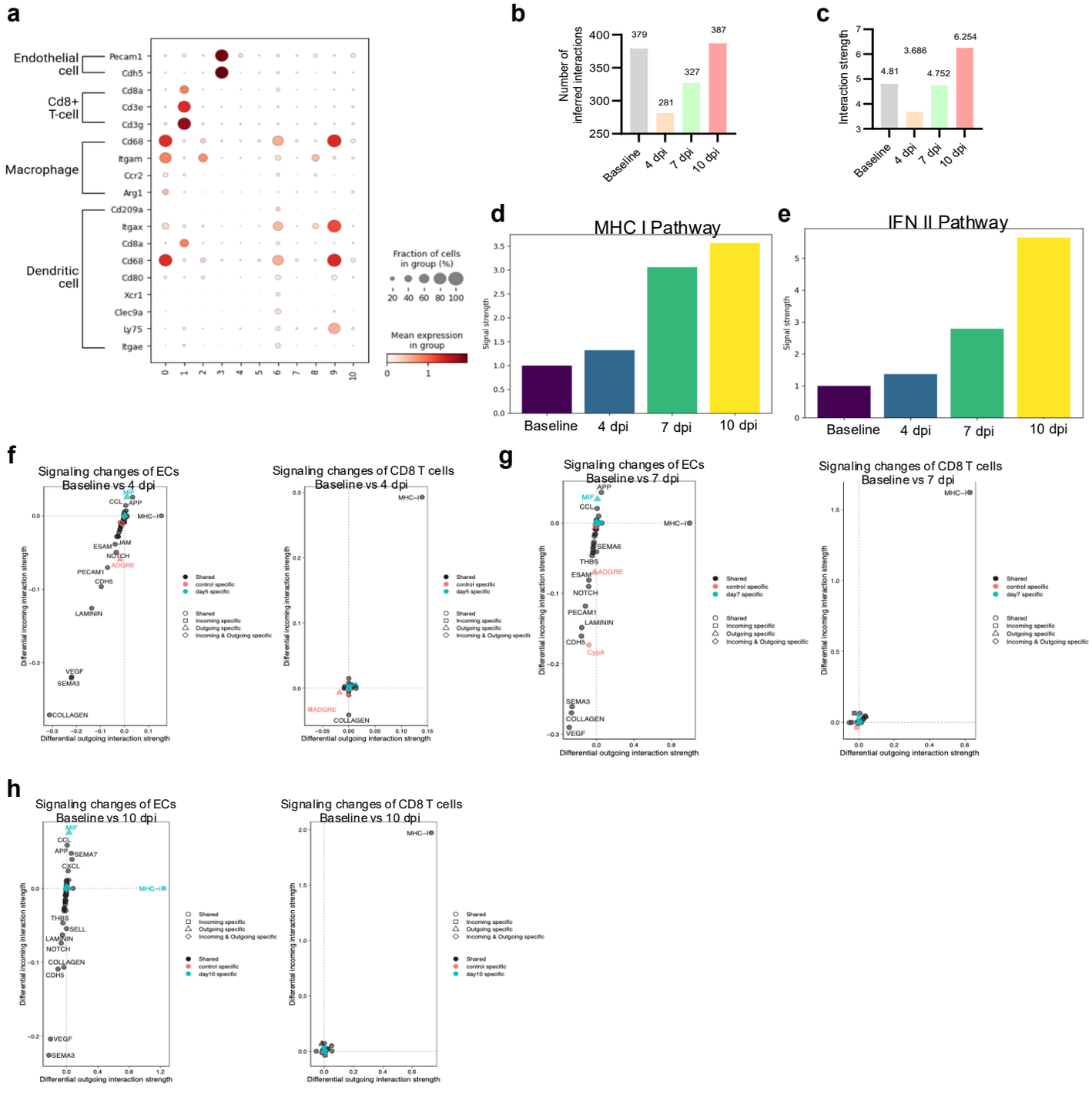

Extended Data Figure 2. Single-cell RNA-seq reveals dynamic EC–CD8⁺ T cell communication during IAV infection. Single-cell RNA-seq analysis of lung cells from C57BL/6 mice at baseline and 4, 7, 10 dpi. (**a**) Cell clusters were annotated by marker genes for endothelial cells, CD8⁺ T cells, dendritic cells, and macrophages. (**b–h**) EC–CD8⁺ T cell communication inferred with CellChat (v2.2.0). (**b**) Number of interactions, (**c**) interaction strength, (**d**) MHC-I signaling strength, and (**e**) IFN-II signaling strength across time points. (**f–h**) Differential signaling at 4, 7, and 10 dpi compared to control (x-axis: outgoing; y-axis: incoming).

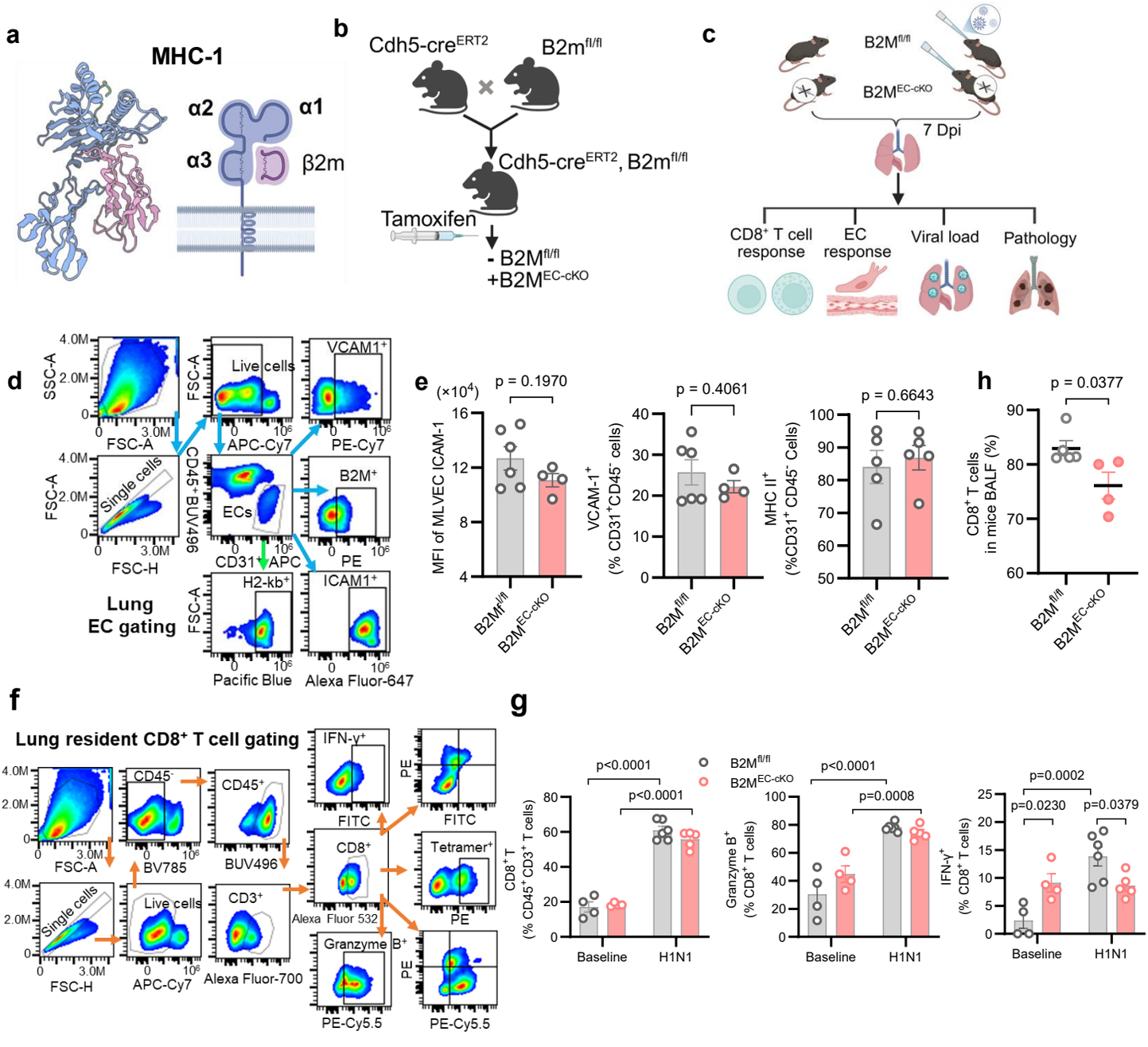

Extended Data Figure 3. Endothelial-specific B2M deletion impairs MHC-I–mediated CD8⁺ T cell responses during H1N1-induced acute lung injury. (**a**) Structural model of the MHC-I complex. (**b**) Strategy for endothelial-specific B2M knockout; tamoxifen-induced Cre given 4 weeks before H1N1 infection. (**c**) Experimental design: $B2M^{EC\text{-}cKO}$ and $B2M^{fl/fl}$ mice infected with 100 PFU H1N1; lungs collected at baseline and 7 dpi for $CD8^+$ T cell, endothelial activation, viral load, and histology. (**d**) Flow cytometry gating of lung ECs for MHC-I, ICAM1, VCAM1. (**e**) MHC-II MFI, $ICAM1^+$, and $VCAM1^+$ PVECs by flow cytometry. (**f**) $CD8^+$ T cell gating for effector (Granzyme B^+, $IFN\gamma^+$) and $tetramer^+$ subsets. (**g**) Lung resident $CD8^+$ T cell effector responses. (**h**) BALF $CD8^+$ T cell analysis. Data are mean ± s.e.m. (≥3 mice). Statistical analysis by unpaired two-tailed t-tests (e-h) and two-way ANOVA (g).

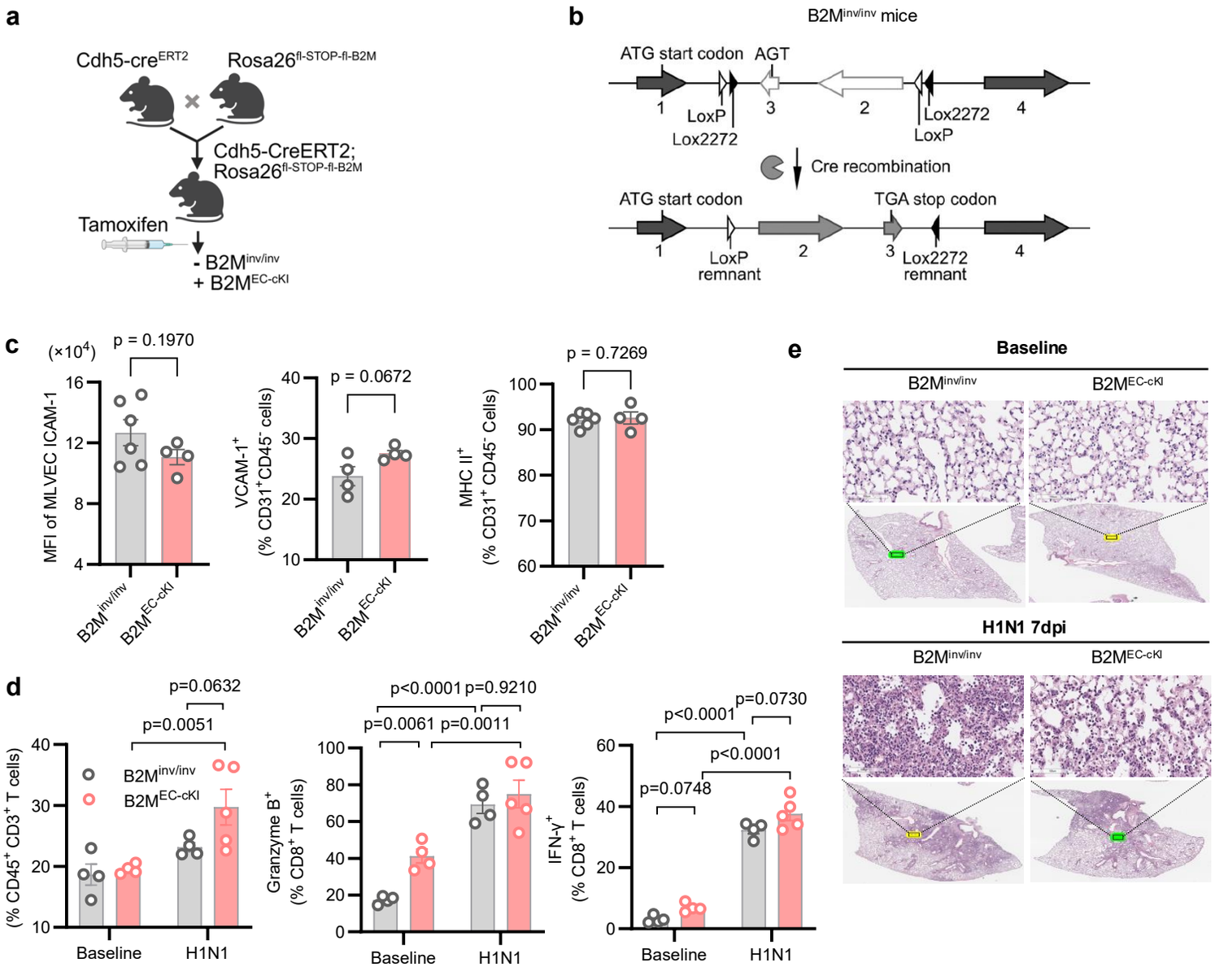

Extended Data Figure 4. Endothelial–specific B2M restoration restore MHC-I expression and enhances CD8⁺ T cell responses during H1N1-induced acute lung injury in vivo. (**a**) Schematic of B2M$^{EC\text{-}cKI}$ mice; tamoxifen restores B2M in ECs. Cre⁻ littermates (B2M$^{inv/inv}$) used as controls. (**b**) Design of B2M$^{inv/inv}$ allele; tamoxifen-induced inversion restores MHC-I on ECs. (**c**) ICAM1 MFI, VCAM1⁺, and MHC-I⁺ PVECs at 7 dpi by flow cytometry. (**d**) Lung resident CD8⁺ T cells and effector subsets (Granzyme B⁺, IFNγ⁺) by flow cytometry. (**e**) Representative H&E lung sections (bottom, full lobe; top, enlarged). Data shown as mean ± s.e.m. (≥3 mice). Statistical analysis by unpaired two-tailed t-tests (c) and two-way ANOVA (d).

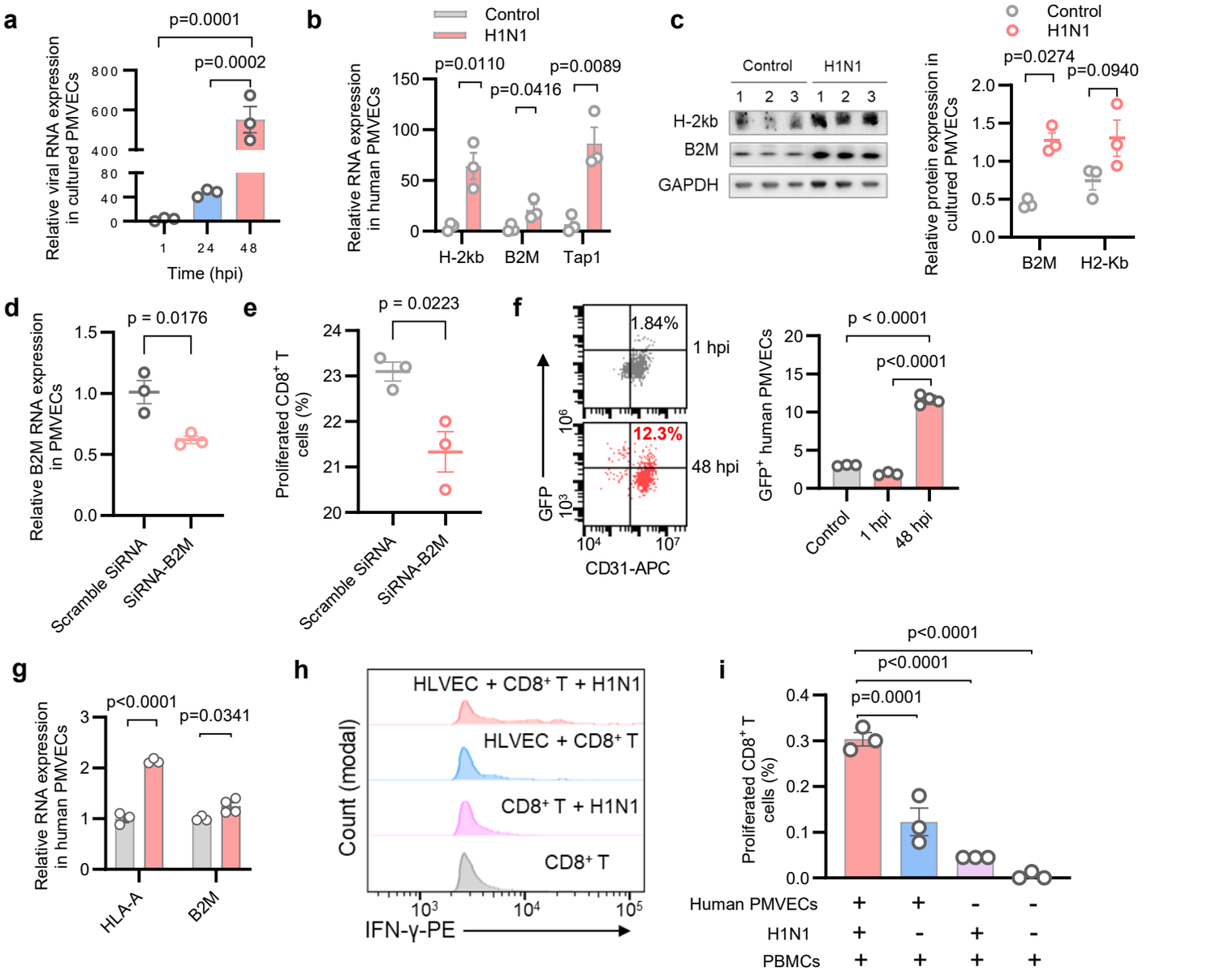

Extended Data Figure 5. In vitro co-culture for PMVECs direct presentation of viral antigen and induce CD8⁺ T cell proliferation and effector responses. (**a**) Viral replication in mouse primary PMVECs infected with H1N1. Cells were harvested at 1, 24, and 48 hpi, and viral NP was quantified by RT-qPCR. (**b**) RT-qPCR analysis of *H2-Kb, B2M, and Tap1* mRNA in PMVECs at 24 hpi, normalized to GAPDH. (**c**) Western blot and quantification of H2-Kb and B2M in mouse PMVECs at 24 hpi versus uninfected controls. (**d–e**) B2M knockdown in mouse PMVECs using siRNA before co-culture; scramble siRNA as control. (**d**) Validation of knockdown by RT-qPCR. (**e**) CD8⁺ T cell proliferation after PMVEC B2M knockdown by flow cytometry. (**f**) H1N1-GFP infection in human primary PMVECs at 1 and 48 hpi by flow cytometry. (**g**) RT-qPCR of HLA-A and B2M mRNA in human PMVECs at 24 hpi, normalized to GAPDH. (**h**) Flow cytometry plots of intracellular IFNγ in CD8⁺ T cells after human peripheral blood mononuclear cells (PBMCs) coculturing with H1N1-infected human PMVECs for 3 days. (**i**) CD8⁺ T cell proliferation after co-culture of H1N1-infected human HLMVECs with PBMCs after 48 h, by flow cytometry. Data represent mean ± s.e.m. from ≥3 biological replicates. Statistical analysis by unpaired two-tailed t-tests (b-e, g) and one-way ANOVA (a, f, i).

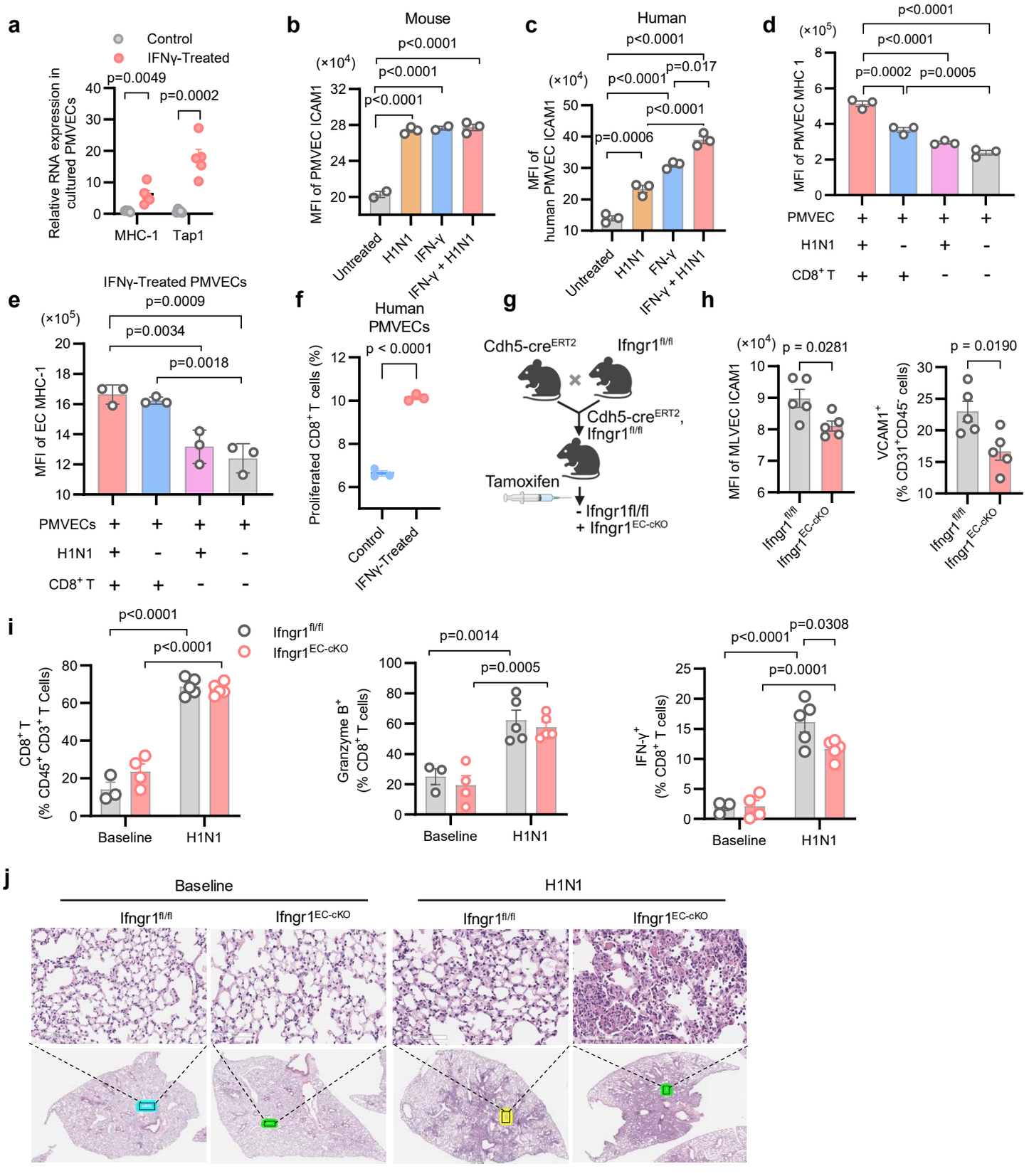

Extended Data Figure 6. IFNγ enhances endothelial MHC-I and adhesion molecule expression and promotes CD8⁺ T cell activation in vitro and in vivo. (**a**) Mouse primary PMVECs treated with IFNγ; MHC-I (H2-Kb) and Tap1 mRNA measured by RT-qPCR (GAPDH as control). (**b–c**) IFNγ-pretreated mouse (**b**) or human (**c**) PMVECs ± H1N1; MFI of ICAM1 on PMVECs were measured by flow cytometry. (**d–e**) H1N1-infected mouse PMVECs co-cultured with CD8⁺ T cells; MFI of MHC I (H2-Kb) quantified on IFNγ-untreated (**d**) or pretreated (**e**) PMVECs by flow cytometry. (**f**) Human PMVECs ± IFNγ, infected with H1N1, co-cultured with CD8⁺ T cells; CD8⁺ T cell proliferation was assessed by flow cytometry. (**g**) Generation of inducible EC-specific Ifngr1 knockout (Ifngr1$^{EC\text{-}cKO}$) mice by crossbreeding Cdh5-Cre^{ERT2} mice with Ifngr1$^{fl/fl}$ mice; Cre-negative littermates as controls. (**h–i**) Flow cytometry detection of PMVEC ICAM1/VCAM1 (**h**) and lung resident CD8⁺ T cell subsets (total, granzyme B⁺, IFNγ⁺) (**i**) in Ifngr1$^{EC\text{-}cKO}$ and controls at baseline and 7 dpi. (**j**) Representative H&E-stained lung sections in Ifngr1$^{EC\text{-}cKO}$ and controls at baseline and 7 dpi. Data are mean ± s.e.m. from ≥3 biological replicates. Statistical analysis by unpaired two-tailed t-tests (a, f, h), one-way ANOVA (b-e), and two-way ANOVA (i).

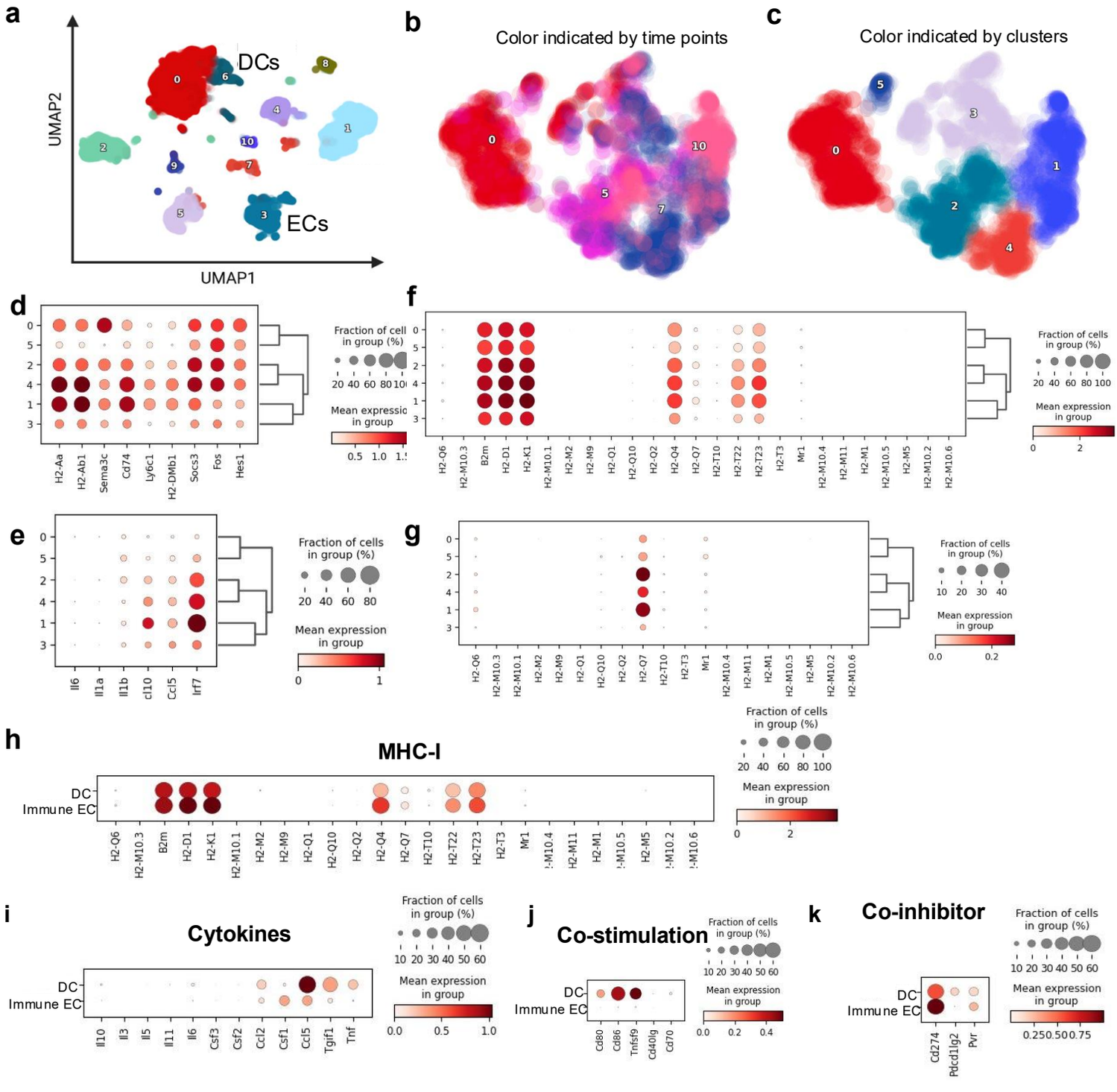

Extended Data Figure 7. Single-cell transcriptomic profiling of PMVEC subsets and immune gene expression post H1N1 infection. Lung cells from C57BL/6 mice were collected at baseline, 4, 7, and 10 dpi for single-cell RNAseq, and PVECs were selected and analyzed. (**a**) UMAP of all lung cells with DCs and ECs identified by cell-specific markers. (**b**) UMAP of PVECs colored by time point. (**c**) UMAP of PVECs showing different clusters. (**d–g)** Bubble plots showing gene expression across six PMVEC clusters: MHC II and regulators (**d**), inflammatory cytokines (**e**), high-expressed MHC I (**f**), and low-expressed MHC I (**g**). (**h–k**) bubble plot to compare gene expression of interests between immune ECs (clusters 1, 2, and 4 based on immune profile) and DCs for MHC I (**h**), inflammatory cytokines (**i**), co-stimulatory molecules (**j**), and co-inhibitory molecules (**k**). Bubble size represents percent of cells expressing a gene; color intensity represents average expression.

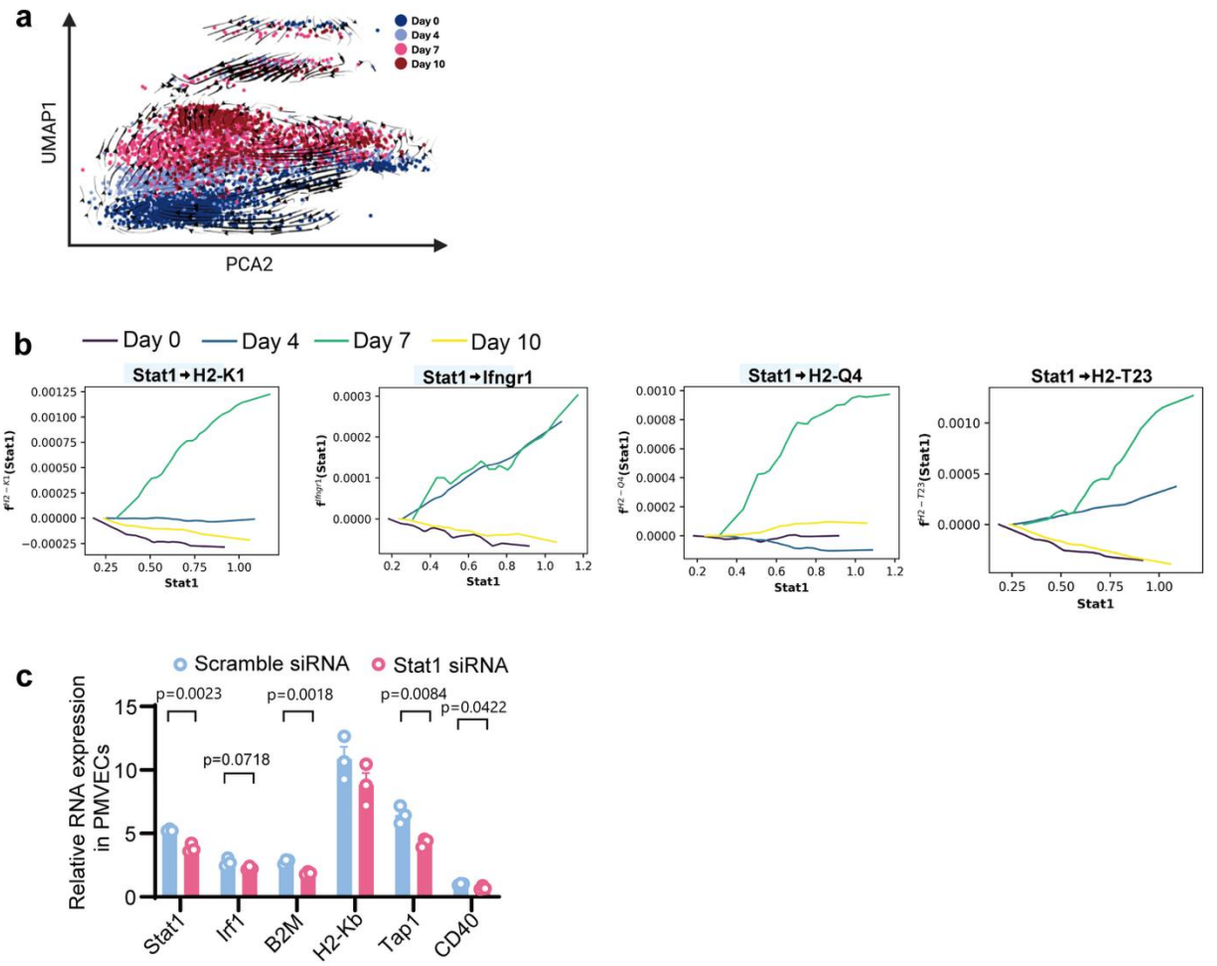

Extended Data Figure 8. IFNγ-STAT1 signaling drives MHC-I upregulation in PMVECs during H1N1 infection. scRNA-seq analysis of PVECs from C57BL/6 mice at baseline, 4, 7, and 10 dpi. (**a**) Instaneous RNA velocity and transcriptional vector field of mixed single PVECs from different time points was reconstructed using Dynamo and GraphVelo to reveal cell-state transition between different time points. This 2D representation (made from a combination of PCA and UMAP axes) depicts time point progression. The reconstructed vector field (all the arrows) projected on to the 2D representation. (**b**) The gene regulatory information was obtained from the velocity vector by Jacobian regulation analysis to reveal how changing the expression of one gene, the regulator, affects the velocity of an effector gene (dose response curve). Cumulative Stat1 regulation over time for H2-K1, Ifngr1, H2-T23, and H2-Q4. (**c**) Cultured PMVECs transfected with Stat1-siRNA or scramble-siRNA; RT-qPCR measured *Stat1, Irf1, H2-Kb, B2M, Tap1, and CD40.* All quantitative data are mean ± s.e.m. from ≥3 biological replicates. Statistical analysis by unpaired two-tailed t-tests (c).

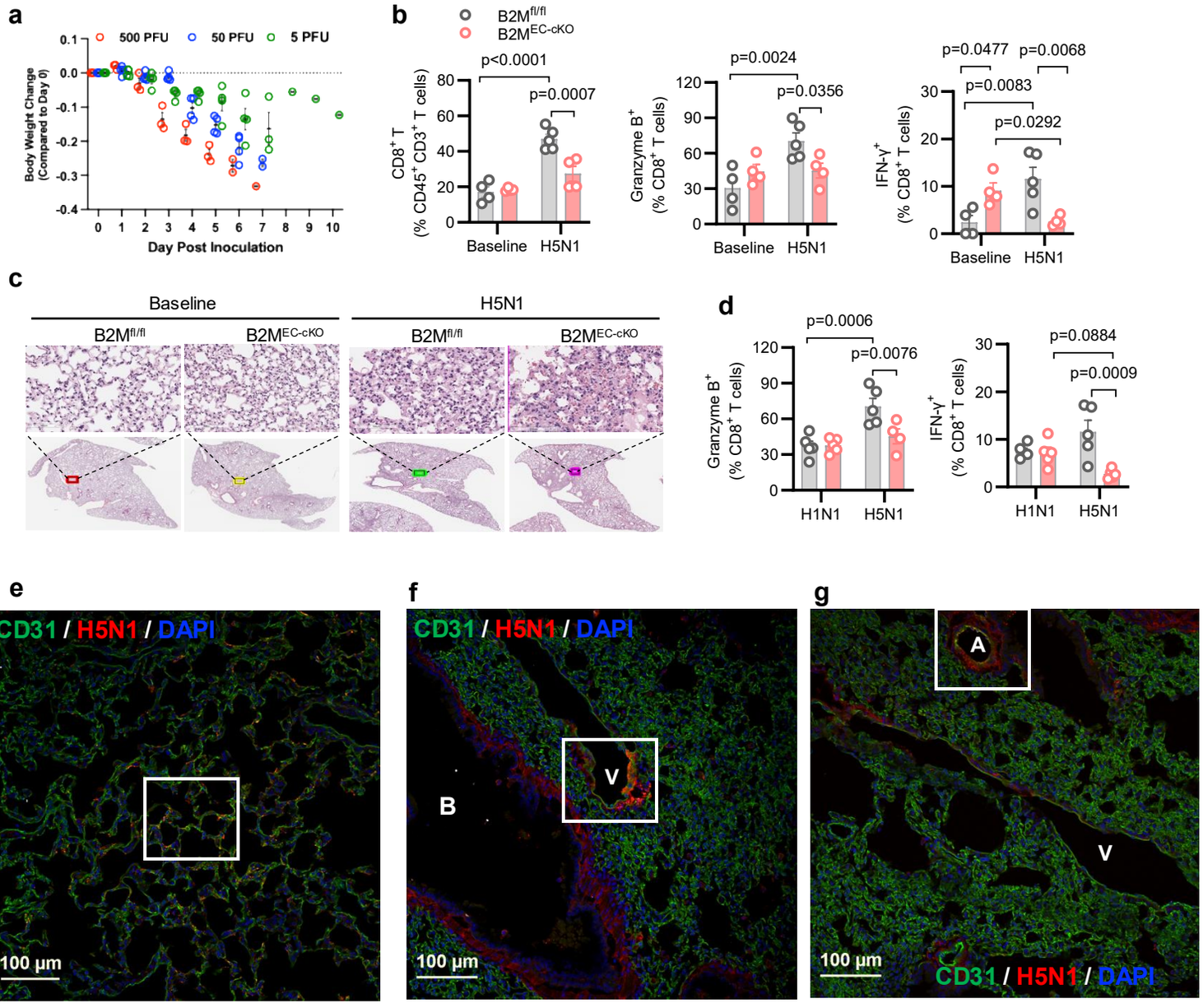

Extended Data Figure 9. Endothelial MHC-I is required for CD8⁺ T cell responses during H5N1 infection. C57BL/6 mice were infected with the highly pathogenic H5N1 strain (A/Texas/37/2024) at 5, 50, or 500 PFU and monitored for 10 days. (**a**) Body weight loss over time. (**b–d**) $B2M^{EC\text{-}cKO}$ and $B2M^{fl/fl}$ mice were inoculated with 5 PFU H5N1 and lungs were analyzed at 6 dpi. Uninfected mice served as baseline controls. (**b**) Flow cytometry of total $CD8^+$ T cells, Granzyme B^+, and $IFN\gamma^+$ $CD8^+$ T cells. (**c**) Representative H&E staining of lung lobes and enlarged regions. (**d**) Comparative $CD8^+$ T cell responses in lungs of $B2M^{EC\text{-}cKO}$ and $B2m^{fl/fl}$ mice infected with 10 PFU H5N1 or H1N1, Lung resident Granzyme B^+ and $IFN\gamma^+$ $CD8^+$ T cells quantified by flow cytometry. (**e–g**) Representative confocal images of lung sections at 4 dpi; white squares indicate zoomed areas shown in **Fig. 6j–i** respectively. A: Arteriole, V: Venule, B: Bronchus. Data are mean ± s.e.m. from ≥3 biological replicates. Statistical analysis by two-way ANOVA (b, d).

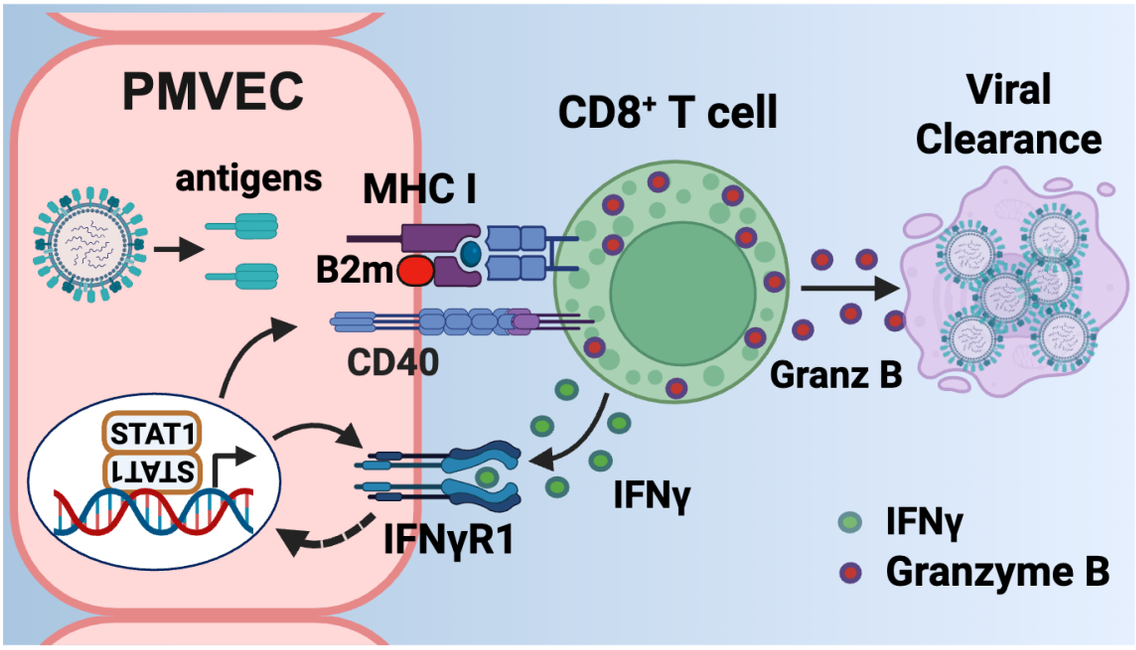

Extended Data Figure 10. Graphic Conclusion